Charge-exchange processes of hydrogen ions with Hg atoms at keV energies

A. van Wijngaarden, J. Patel, K. Becker,* and G. W. F. Drake
Department of Physics, University of Windsor, Windsor, Ontario, Canada N9B 3P4
(Received 5 March 1985)

A search for the production of the $2p^2\ ^3P^e$ state of H^- has been made by crossing a $H^-(1s^2)$ ion beam of energies $E<140$ keV with a thermal Hg beam inside a static electric field. The formation of $H^-(2p^2)$ ions and their subsequent decay to neutral $H(1s)$ results in a feature on the angular distribution of the neutral particles produced in electron loss of the ground-state $H^-(1s^2)$ ions. The absence of such a feature sets an upper limit of 10^{-20} cm^2 to the cross section for formation of the $2p^2\ ^3P^e$ state. Differential (with respect to angle) charge-transfer cross sections for scattering in the angular range $3°<\theta<15°$ as well as the small-angle forward cross sections σ_{10} and σ_{-10} for hydrogen ions passing through Hg vapor are presented.

I. INTRODUCTION

The H^- ion has but two bound states. The $1s^2\ ^1S_0$ ground state is well known[1] but the properties of the $2p^2\ ^3P^e$ excited state predicted by Drake[2] and confirmed by Jacobs *et al.*[3,4] have not been firmly established experimentally. The state has a binding energy of 0.0095 eV and spontaneously decays according to

$$H^-(2p^2)\rightarrow H(1s)+\hbar\omega+e^- \quad (1)$$

with a lifetime $\tau=1.73\times10^{-9}$ sec. Upon decay, the excitation energy is shared between the photon and the electron. This state is the only known atomic state where the energy is partitioned among the decay products and the decay mechanism leads to a broad spectral feature on the long-wavelength side of Ly-α.

Although the satellite observation[5] of a tail on the Ly-α frequency distribution in stellar atmospheres suggests the existence of the $2p^2$ H^- state, attempts to observe it under controlled laboratory conditions[6,7] have failed. This paper describes an attempt to detect the state by observing the $H(1s)$ decay product. In the experiment a highly collimated beam of ground-state H^- ions crosses a thermal beam of Hg atoms inside a static electric field. The $2p^2$ H^- ions that are presumably formed in (glancing) collisions with the Hg atoms survive a sufficiently long time (τ) as charged particles to be noticeably deflected by the field before decaying to the neutral state. The decay in flight of the $2p^2$ H^- ions results in a feature on the angular distribution of the neutral particles formed by direct neutralization of the ground state $1s^2$ H^- ions.

Though no evidence for the production of $H^-(2p^2)$ ions was found, it was possible to set an upper limit to this process. Furthermore, the observed angular distributions of the neutral particles at a large distance from the overlap region of the crossed beams allowed us to deduce the σ_{-10} cross section for ground-state $H^-(1s^2)$ ions. Similarly, with proton beams, the σ_{10} cross section was measured.

Charge transfer of hydrogenic ions in various media is of practical interest for accelerators and for neutral-particle beam injection into plasmas for the fusion energy program. An extensive body of literature has been summarized in the review by Tawara and Russek.[8] Most of the earlier transfer cross sections have been measured for gases, followed by those for the alkali halides, and more recently for the alkaline earths.[9,10]

To our knowledge no data exist for the transition elements, and the charge-transfer cross sections in Hg reported in this paper have not been previously measured. A detailed understanding of charge transfer of single electrons in glancing collisions is lacking. Since corresponding theories at best reproduce the forward cross sections over a typical energy range of 10—100 keV within a factor of 2, we have limited our study for σ_{-10} and σ_{10} to a purely experimental one.

Our crossed-beam technique may readily be extended to other high-Z targets. It has the advantage over the gas-cell targets that single-collision conditions for a low-density thermal beam are guaranteed. In conventional experiments the ion beam is made to traverse a long gas cell. It is then assumed that single-collision conditions prevail when the pressure of the gas cell is reduced to a region where the yield of a given charge component is proportional to pressure. However, the linearity is not a sensitive enough test[11] when competing secondary cross sections are large.

Section II describes the apparatus for the ion beam, the thermal Hg beam, and the measurement of target thickness by Rutherford scattering. A search for the $2p^2\ ^3P^e$ H^- state is described in Sec. III. Charge-transfer measurements for both large- and small-angle scattering are presented in Sec. IV and finally, a discussion of the results is given in the last section.

II. EXPERIMENT

A. Overall plan

A schematic diagram of the apparatus is shown in Fig. 1. A collimated beam of H^- ions obtained from a $\pi/2$ magnetic analyzer crosses a thermal beam of Hg atoms inside a static electric field maintained between two parallel plates. The field separates the main H^- component from the neutral particles. At a distance of 86.0 cm from the interaction region a Faraday cup located at a nominal

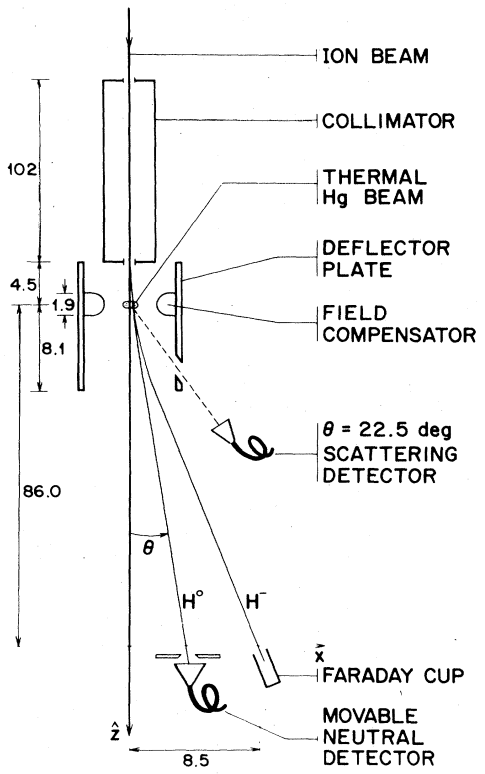

FIG. 1. Schematic diagram of the apparatus (not to scale) with dimensions in cm.

(maximum) transverse distance $x=8.5$ cm, corresponding to a deflection angle $\theta=5.7°$ monitors the incident ion beam.

Figure 2 shows that there are two components of neutral particles after the ion beam crosses the Hg beam. The undeflected large component centered at $\theta=0°$ arises from charge transfer with the residual gas (5×10^{-7} Torr) inside the collimator. The other centered at $\theta=1.33°$ results from charge transfer with the thermal Hg beam. Its intensity is a factor of 10^2 smaller than that for the $\theta=0°$ profile. When the Hg beam is switched off, the $\theta=1.33°$ distribution disappears. The separation of the two neutral components is essential if the symmetry of the $\theta=1.33°$ profile is to be measured accurately.

B. Hg beam

Figure 3 shows the thermal Hg gun and its positioning relative to the ion beam. The thermal vapor jet is produced by allowing vapor from a heated reservoir to pass through an array of densely packed hypodermic needles. Each needle is 1 cm long and has a diameter of 0.031 cm. The length of the array along the ion beam direction is $l=0.318\pm0.003$ cm and its width is 0.76 cm. The ion beam itself has a circular cross section of 0.1 cm diam and just passes underneath the needles at a distance of 0.3 cm. A heating element is wound around the 1.3-cm-diam stainless-steel pipe holding the needles, and the temperature of the Hg reservoir is kept stable to within 0.01 °C with the aid of a thermistor.

A Teflon plunger mounted on a bellows system acts as a shutoff valve. Closing it reduces the Hg vapor flow by a factor of 50, in a time interval of a few seconds. The Hg vapor is ultimately condensed into a liquid-N_2-cooled trap just below the parallel plates. The residual gas pressure in the interaction region is 6×10^{-8} Torr.

To ensure a small angular divergence of the vapor jet, the Hg temperature was kept as low as possible. The effective length of the interaction region began to increase noticeably only at temperatures above 50 °C, as evidenced by the onset of an increase in the angular width of the distribution of the neutral particles [see Eq. (2) of Sec. II C]. While at a temperature of 25 °C the atomic density in the Hg beam is still sufficiently high to produce an adequate signal of neutral particles, the density was too small to be measured by Rutherford scattering (Sec. II E). A Hg temperature of 35.5 °C was chosen as a compromise and at these low densities the effective length is nearly the same as the width ($l=0.318$ cm) of the needle array.

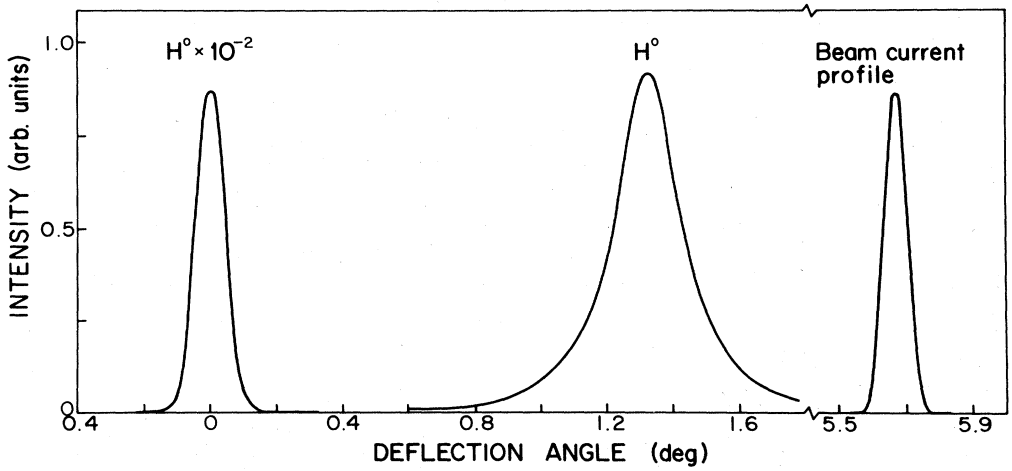

FIG. 2. Angular profiles. The distribution centered at deflection angle $\theta=0°$ represents the neutral component in the primary H^- beam. The distribution centered at $\theta=1.33°$ is for neutral particles produced in charge transfer with the thermal Hg beam. The scale for the two neutral distributions is the same but differs from that for the beam-current profile centered at $\theta=5.7°$, for a typical beam current of 2×10^{-10} A.

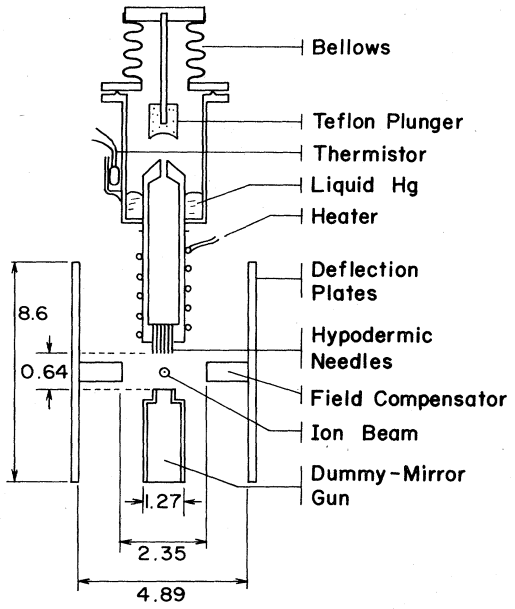

FIG. 3. Schematic diagram of the Hg gun (not to scale) and its positioning relative to the ion beam. Dimensions are in cm. The gun and its mirror image are kept at ground potential while the deflector plates have opposite polarities.

C. Detection and angular profiles

The neutral particles are detected with a Channeltron detector. Its rectangular entrance slit of width $\Delta x = 0.094 \pm 0.002$ cm, corresponding to an acceptance angle $\Delta\theta = 0.0626°$ and height of 0.96 cm, was covered with a thin Al film that stops low-energy particles but is yet sufficiently thin that hydrogen ions of keV energies have a detection efficiency of nearly 100% (see Ref. 12, and references therein).

Angular distributions for the neutral components are obtained by monitoring the Channeltron output counts as it is moved along the x direction in Fig. 1. The angular profile of the neutral particles near $\theta = 0°$ is of Gaussian shape with a full width at half maximum (FWHM) of 0.102°. The corresponding width for the Gaussian distribution of the incident ion beam, normally centered at $\theta = 5.7°$ is 0.079°. The ion-beam profile was measured by temporarily placing a rectangular slit in front of the Faraday cup with dimensions identical to that of the entrance slit of the Channeltron and by scanning the cup across the beam. Because of the finite energy spread of one part in 600 in the incident beam, the angular width depends weakly on the electric field between the parallel plates and it decreases from 0.079° to 0.075° when the electric field is switched off.

The difference in angular width of nearly 0.02° between the $\theta = 0$ distribution and that for the incident ion beam can be accounted for by charge-changing collisions inside the collimator. During such collisions the deflection angle of keV H^- ions at speeds comparable to the Bohr velocity ($v_0 = 2.2 \times 10^8$ cm/sec) is of order 10^{-2} deg.

The angular width for the distribution of neutral particles formed in charge transfer with Hg atoms depends on the angular width of the incident ion beam as defined by the collimator and on the thickness l (0.318 cm) of the Hg beam along the path of the projectiles. The field-induced increase in angular spread, with charge neutralization taking place uniformly along the overlap distance while the primary ion beam is being deflected by the electric field, is given by

$$\Delta W(\mathrm{FWHM}) = Fl/2V_a \ . \tag{2}$$

Here F is the electric field at the site of the interaction region whose value is proportional to the plate potential V_p, and V_a is the accelerating potential. Thus the angular width at finite fields is given by the sum of the field-free width and the field-induced spread

$$[W(\mathrm{FWHM})]_F = [W(\mathrm{FWHM})]_0 + Fl/2V_a \ . \tag{3}$$

D. Electric field

Insertion of the stainless-steel needle holder between the parallel plates adds nonuniform vertical components to the electric field. This adversely affects the symmetry of the angular distribution of the neutral particles in the observation region. Restoration of the field symmetry was accomplished by mounting a mirror "dummy gun" (see Fig. 3). Two field compensators were installed to raise the field to a sufficiently high level in the interaction region.

Since a field calculation for our geometry is very tedious, it was determined, instead, from a measurement of the field dependence of ΔW(FWHM). The latter was found to be proportional to V_p/V_a, in agreement with Eq. (2), in the range $3.5 \times 10^{-2} < V_p/V_a < 7.0 \times 10^{-2}$ studied, and yields

$$F(\mathrm{V/cm}) = (0.219 \pm 0.005) V_p \ (\mathrm{V}) \ . \tag{4}$$

The precision has been limited by the finite range for V_p/V_a. The lower limit is the one where the H^0 distribution from charge transfer with Hg atoms begins to overlap with the distribution of neutral particles in the primary beam (see Fig. 2). The upper limit is determined by the largest accessible deflection angle $\theta = 5.7°$ (see Sec. II A). Substitution of the known field values given by Eq. (4) into Eq. (3) allows a determination of the field-free angular width of the neutral particles. For H^- and H^+ projectiles, the resulting field-free widths of $0.087° \pm 0.002°$ and $0.090° \pm 0.002°$, respectively, both exceed the angular width $0.079° \pm 0.002°$ for the incident ion beam by about 0.01°. Such a difference can reasonably be attributed to the angular divergence resulting from charge transfer.

E. Measurement of target thickness

The determination of an absolute cross section requires a measurement of the product Nl of the average number density N in the target medium and the effective overlap distance l of the interaction region. We obtained this quantity from the Rutherford scattering yield for protons at large scattering angles.

Since Rutherford scattering is highly peaked forward, the yield at angles $\theta > 30°$ became too small for the signal to lie significantly above the noise level. Background noise arises from slit-scattered particles and from scatter-

ing with residual gas (6×10^{-8} Torr) in the interaction region. On the other hand, for small scattering angles $\theta<10°$, electronic screening of the target nucleus becomes so severe that theory in this region may not be reliable enough for a precise calibration. It is known,[12] however, that Thomas-Fermi differential scattering cross sections $d\sigma/d\Omega$ for scattering of keV hydrogenic projectiles from Hg at $\theta\gtrsim20°$ account well for screening and should fall within a 10% confidence level. The Channeltron mounted at a distance of 9.517 cm from the Hg beam at a scattering angle $\theta=22.5°\pm0.2°$ (see Fig. 1) is the calibration detector. The solid angle subtended to the interaction region is

$$\Delta\Omega=(6.85\pm0.04)\times10^{-3}\text{ sr}\ . \tag{5}$$

To reduce noise counts from multiply scattered low-energy particles, its entrance aperture is covered with a self-supporting Al film. The angular distribution of the Hg-scattered particles over the large acceptance angle $\Delta\theta=5.35°$ can no longer be considered uniform. Taking into account that at energies $E<40$ keV the angular distribution varies approximately as $\sin^{-3}(\theta/2)$, the effective scattering angle becomes $\theta=22.19°$.

We now define the scattering yield Y as the ratio of the particle current scattered into the solid angle $\Delta\Omega$ to the incident projectile current. Hence

$$Y=\left[\frac{d\sigma}{d\Omega}\right]_{\text{sc}}\Delta\Omega(Nl) \tag{6}$$

and a measurement of Y is equivalent to a measurement of Nl. The yield was determined from the difference in counting rate with the Hg beam turned on and off. Though the signal-to-noise ratio was as low as 1.5, Y values were determined with an adequate statistical precision of $\pm5\%$ over a small energy range.

Multiplication of the yields by the normalizing factor 3.324×10^{-9} puts them onto the solid curve in Fig. 4

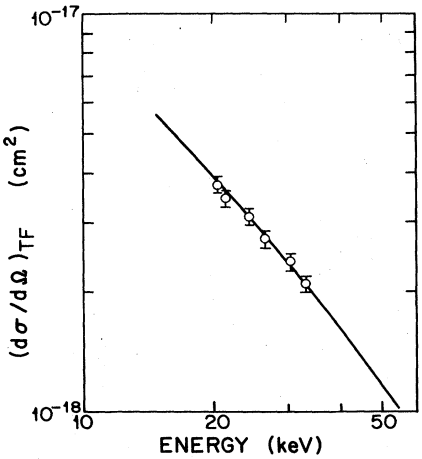

FIG. 4. The energy dependence of the Thomas-Fermi differential scattering cross section for the scattering of hydrogen projectiles from Hg atoms at a scattering angle $\theta=22.19°$. Points are the observed scattering yields (see text) multiplied by 3.324×10^{-9}. Error bars are explained in the text.

which represents the energy dependence of the Thomas-Fermi scattering cross section[13] for a scattering angle $\theta=22.19°$. Thus

$$\frac{d\sigma}{d\Omega}=3.324\times10^{-9}Y\ . \tag{7}$$

The error in the points include the error from counting statistics ($\sim5\%$), the error of 0.6% in $\Delta\Omega$, and a 3% error in the primary beam flux. Comparing Eq. (7) with Eq. (6) and using Eq. (5) gives the desired result

$$Nl=(4.39\pm0.17)\times10^{10}\text{ atoms/cm}^2\ . \tag{8}$$

This target density is equivalent to a target thickness equal to 10^{-5} of a monolayer, sufficiently thin that single-collision conditions prevail in our measurements of the charge-transfer cross sections.

III. SEARCH FOR $2p^2\ {}^3P^e$

A. Experimental method

To form the $2p^2$ H^- state one might be tempted to use protons in charge-changing collisions involving double-electron capture. During such a reaction, however, the target obtains a positive charge which can result in a sufficiently strong electric field at the site of the hydrogenic projectile to prevent the development of the state. In fact, since the radius of the state is of order $20a_0$ and the binding energy only 0.0095 eV (Ref. 2) it can readily be seen that fields $F\gtrsim10^5$ V/cm cannot be supported by the system.

In our attempt to create the state in glancing collisions of ground state $H^-(1s^2)$ ions with Hg atoms, the harmful effects from a charged target are eliminated. The resulting $H^-(2p^2)$ ions decay in flight and contribute to the σ_{-10} transfer cross section. Their deflection by the external electric field results in an exponentially shaped feature of neutral particles that will be superimposed on the larger-angle-deflection side of the bell-shaped H^0 profile from the ground state H^- ions. The resulting asymmetry should be noticeable for several half-widths away from the center. This is because for a lifetime $\tau=1.73\times10^{-9}$ sec and a typical beam velocity $v=4\times10^8$ cm/sec, the decay length $v\tau=0.69$ cm is more than double the length of the interaction region.

One can now extract the exponential part of the bell-shaped H^0 distribution, centered at θ_0, by subtracting the intensities $I(\theta-\theta_0)$ for negative arguments from the corresponding ones for positive arguments. A plot of this difference versus $\Delta\theta=\theta-\theta_0$ on a semilogarithmic scale can be made. The resulting straight line for $\Delta\theta$ greater than the half-width of the H^0 profile should have a slope

$$s=-(Mv/eF)\tau\ . \tag{9}$$

B. H^0 angular profile

The upper and lower curves in Fig. 5 are the angular distributions of neutral particles with the Hg beam switched on and off, respectively. The incident beam consists of $H^-(1s^2)$ with an energy of 134 keV. Such sets of curves were obtained at several energies for a constant ra-

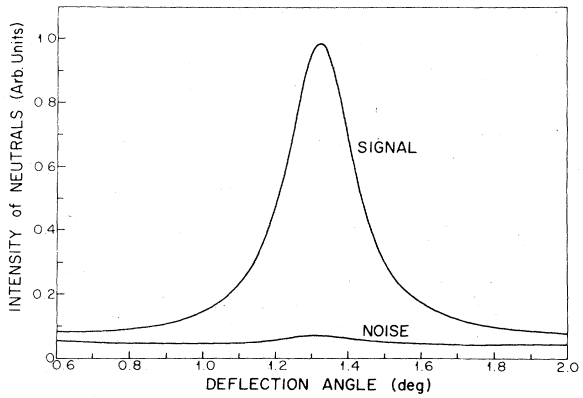

FIG. 5. Angular profile of neutral particles produced in electron loss of 134-keV H^- ions in passing through Hg vapor. The upper and lower curves were obtained with the Hg beam switched on and off. The signal profile is similar to the $\theta=1.33°$ distribution in Fig. 2.

tio of plate to accelerating potential. Under this condition the overall shape of the curves were found to be independent of energy. The curves were obtained with the angular interval divided into 40 equal parts and collecting signal counts at each angular position for precisely equal counting periods. The total number of signal counts for a curve is of the order of 1 to 2 million and points in the wings contain at least 7×10^3 counts each. Since errors from counting statistics alone are negligibly small, only a smooth curve drawn through the points is exhibited, not the points themselves. The signal that remains after subtracting the noise curve is a non-Gaussian bell-shaped curve with pronounced wings. The signal in the wings has its origin in the divergence of the Hg beam. The fact that the field-free $(FWHM)_0$ of these curves (see Sec. II D) yield the approximate angular width of the incident beam (Sec. II C) indicates that in spite of the Hg beam divergence, the effective interaction length l remains well defined. At larger angles from the center, greater than five half-widths, a small signal remains which smoothly joins the angular distribution for large-angle scattering.

C. Asymmetry and conclusion

When one of the bell-shaped H^0 distributions contains a total of several million counts, the statistics becomes adequate to test for very small asymmetries. Indeed one finds more counts in the wing for larger angular deflections than in the other wing. The asymmetry approximately has exponential behavior over a small angular range, but the decay is independent of beam velocity in violation of Eq. (9). Furthermore, the asymmetry remained when the H^- projectiles were replaced by either a proton or an H_2^+ ion beam. The presence of the asymmetry, therefore, does not arise from the decay of $H^-(2p^2)$ ions but is a purely instrumental effect.

Qualitatively we could account for it from a study of the beam profile of our $\pi/2$ magnetic analyzer. The analyzer, through its focusing action, produces a nonuniform intensity distribution across its exit slit which makes the H^0 distribution inherently asymmetric.

Thus no evidence of $H^-(2p^2)$ ions was found. From a statistical analysis of the data we find that our search would have been successful if the cross section for forming the $2p^2\,{}^3P^e$ state in collisions of $H^-(1s^2)$ ions with Hg atoms were as small as 10^{-20} cm^2.

It is apparent that the cross section for the excitation of two electrons from the $1s^2$ to the $2p^2$ configuration is very small. In the absence of theoretical prediction, we speculate that the Hg atom with its many electronic states in momentum space is a more favorable target than the Ar target of Risley *et al.*[6] and Berry.[7] A disadvantage of our search is that it required a finite electric field of 1000—1500 V/cm. Although such a field will not destroy the state by field ionization, the lifetime may be reduced by tunneling. For the unlikely event that such a mechanism would lower the lifetime by more than a factor of 5, our technique would have been ineffective.

IV. CHARGE TRANSFER FOR HYDROGEN IONS

A. Cross section

When a beam of charged hydrogen projectiles passes through a thin target of small density with Nl atoms/cm^2 such that single collisions prevail, the fraction of neutral particles in the emerging beam is given by

$$f=Nl\sigma_0\,. \tag{10}$$

This equation is considered to be the operational definition for the neutralization cross section σ_0. The definition is somewhat arbitrary. The beam in traversing the medium diverges as a consequence of screened Rutherford scattering and our definition does not specify the angular range over which the neutral-particle content should be measured. In practice, however, the scattering is highly peaked in the forward direction and as shown in Sec. II D the vast majority of neutral particles lie within an angular scattering range $0<\theta<0.2°$, so that the discrepancy between the forward σ_0 cross section and the total cross section taking into account all scattering angles is small, but not negligible. The discrepancy may be estimated from a study of the differential transfer cross section $d\sigma_0/d\Omega$ at larger scattering angles.

B. Charge transfer at large angles

In an earlier investigation[12] we measured the scattering cross sections $(d\sigma/d\Omega)_{sc}$ for hydrogen projectiles with Hg atoms for large angular deflections, a cross section which is independent of the charge state of the incident ion at keV energies. We also measured large-angle charge-transfer cross sections that were not published but are presented here.

The apparatus was similar to that in Fig. 1 with the parallel deflection plates removed. Instead, an electric field transverse to the direction of motion of the Hg-scattered projectiles, just in front of the scattering detector, could be switched on to remove charged components from the scattered beam. The fraction P_0 of scattered neutral particles was then obtained by monitoring the output signal from the detector with the field switched on and off. Thus

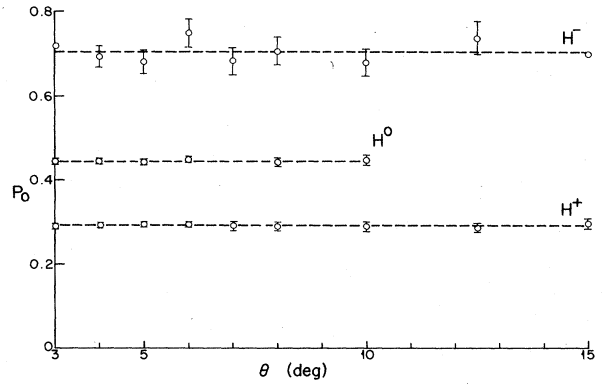

FIG. 6. Angular dependence of the fraction P_0 of neutral particles in Hg-scattered hydrogen projectiles for three incident beams of H^-, H^0, and H^+ projectiles at an energy near 40 keV. Lines pass through the angle-averaged experimental points. Error bars are explained in the text.

$$P_0=\left[\frac{d\sigma_0}{d\Omega}\right]\Big/\left[\frac{d\sigma}{d\Omega}\right]_{sc}, \tag{11}$$

where $d\sigma_0/d\Omega$ is the differential charge-exchange cross section for formations of neutral particles.

The labels H^-, H^0, and H^+ in Fig. 6 refer to the charge state of the incident ions. The figure shows the angular dependence of P_0 for each at the beam energy $E\simeq 40$ keV. The angular dependence was measured with a rather poor resolution $\Delta\theta=1°$ and under this condition the P_0 values are within experimental error independent of θ in the range $3°<\theta<15°$ studied. The error bars on the points arise from counting statistics and fluctuations in beam current. Errors for H^+ and H^0 are smaller than those for H^-. The relatively small H^- primary beam current required an average counting period of a few hundred seconds for each point. Horizontal lines have been drawn through the experimental points to determine the average P_0 values at a given energy. The energy dependence of P_0 is shown in Fig. 7. Thomas *et al.*[14] also found an angular independence of P_0 for scattering angles in the range $0.5°<\theta<10°$ of hydrogen projectiles in various gases.

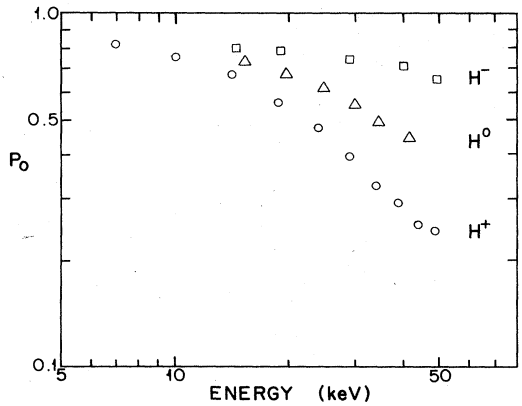

FIG. 7. The energy dependence of P_0 for H^-, H^0, and H^+ projectiles after scattering from Hg atoms. Errors bars are of the same magnitudes as the points and too small to indicate.

One might speculate about the significance of the angular independence. Just prior to a collision, the projectile has a specific charge state which becomes undefined during the collision. That the final charge state is independent of scattering angle shows the relative importance of the postcollision evolution of the final charge state, after scattering. In view of this, the ordering for the relative magnitudes of P_0 in Figs. 6 and 7 is not surprising. The more positively charged the incident projectile, the fewer electrons will be available for capture as the proton emerges from its Hg scattering center.

The concept of a postcollision evolution of the charge state is meaningful only for light projectiles. Thus although we found that for keV He^+ projectiles, P_0 is also independent of scattering angle, for N^+ projectiles it decreases rapidly with increasing θ. This behavior is expected. For large-Z projectiles the final charge state depends on the excitation of the inner electrons during the collision.

An estimate of the charge-transfer cross section for angles $\theta>1°$ can now be obtained. For example, for 50 keV hydrogen in scattering from Hg with deflections $1°<\theta<20°$, the scattering cross section is approximately given by[12]

$$\frac{d\sigma}{d\Omega}\sin^3\left[\frac{\theta}{2}\right]\simeq 1.2\times 10^{-20}\ \text{cm}^2\ . \tag{12}$$

Though deviations from this equation become appreciable at $\theta>20°$, the larger-angle collisions contribute but little to the total scattering cross section and the previous equation may be used to estimate the total scattering cross section for $\theta>1°$. On substitution of Eq. (12) into

$$\sigma_{sc}(\theta>1°)\simeq\int_{1°}^{180°}\frac{d\sigma}{d\Omega}2\pi\sin\theta\,d\theta$$

one obtains $\sigma_{sc}(\theta>1°)\simeq 1.7\times 10^{-17}$ cm^2. At our energy of 50 keV, $P_0=0.25$ for protons (see Fig. 7) and the charge-transfer cross section is seen to be $\sigma_{10}(\theta>1°)\simeq 4.3\times 10^{-18}$ cm^2, nearly 2% of the forward σ_{10} ($\sim 2\times 10^{-16}$ cm^2) for $\theta<1°$ (see next section).

C. Forward charge-transfer cross section

To find the charge-transfer cross section, a knowledge of the fraction of neutral particles in the beam after it emerges from the Hg vapor is required. The total number of neutral particles for an H^0 distribution, such as the one shown in Fig. 5, is given in principle by the area between the signal and the noise curves. However, this area is a

TABLE I. Observed charge-transfer cross sections of hydrogen ions in Hg. (a) σ_{10} for electron capture by protons. (b) σ_{-10} for electron loss by H^- ions.

Energy (keV)	Cross section (10^{-16} cm^2)
(a)	
23.8±0.2	6.70 ±0.38
28.0±0.3	5.12 ±0.29
35.5±0.4	3.49 ±0.20
47.0±0.5	2.29 ±0.13
59.5±0.6	1.63 ±0.09
73.4±0.7	1.21 ±0.07
93.8±0.9	0.900±0.051
109.5±1.1	0.712±0.040
124.4±1.2	0.624±0.035
134.5±1.4	0.544±0.031
(b)	
31.0±0.3	10.03±0.57
41.3±0.4	10.71±0.61
54.7±0.5	11.34±0.64
73.4±0.7	11.40±0.65
93.2±0.9	11.50±0.65
114.0±1.1	10.54±0.60
134.2±1.3	10.05±0.57

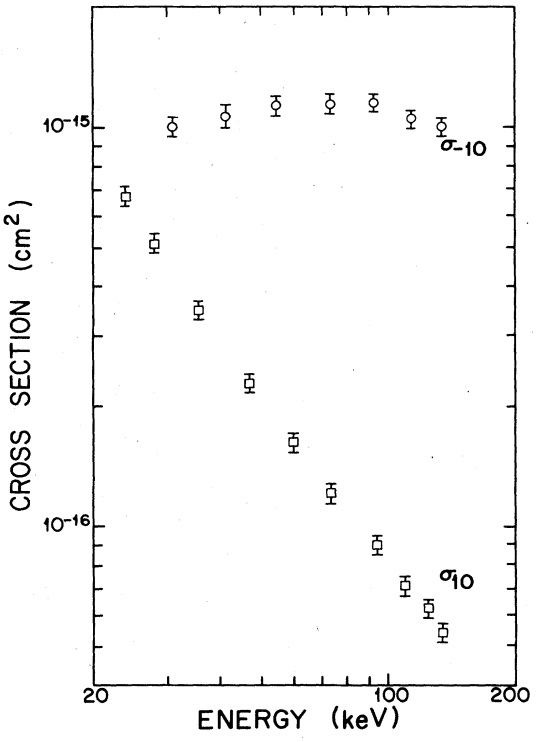

FIG. 8. The energy dependence of the charge-transfer cross sections σ_{-10} and σ_{10} for hydrogen projectiles in Hg. For an explanation of error bars, see text.

true measure of only those neutral particles that enter the entrance slit (0.094 cm×0.955 cm) of the detector as it is scanned along the x observation axis. The solid angle for this detector is $(1.214\pm0.033)\times10^{-5}$ sr. Particles that scatter in the y-z plane through angles larger than half of the angle (0.321°) subtended by the slit height are excluded from observation. In this plane, the angular divergence of the neutral particles is not widened by the electric field and the angular full width is given by the zero field value of 0.09° (see Sec. II D), which is seven times smaller than the angle subtended by the slit height of 0.642°.

Integration along the observation axis was carried out over a range of 2.5 full widths, equal to 0.57° on either side of the maximum of the distribution (see Fig. 5). This large interval is necessary because of the pronounced scattering wings produced by the product [see Eq. (2)] of the Hg beam divergence and the electric field. We estimate that the finite limits of integration underestimate the resulting charge-transfer cross sections over an actual angular scattering interval of $0°<\theta<0.2°$ by less than 2%.

The charge-transfer cross section can now be found using $\sigma_0=f/Nl$ [Eq. (10)] where $Nl=4.39\times10^{10}$ cm^{-2} [Eq. (8)]. The cross sections σ_{-10} and σ_{10} have been tabulated in Table I and summarized in Fig. 8. Each error bar results from a combination of the errors in target thickness (4.0%), projectile beam flux (3.0%), the solid angle of the detector (2.7%), and an integration error which varies from one measurement to another but has an average value of 0.3%. Whereas the relative precision of the measurements lies within ±6%, the absolute cross sections only fall within the 15% precision level in view of the theoretical uncertainties in the Thomas-Fermi cross sections used for calibration.

V. DISCUSSION

Earlier attempts to detect the $2p^2\,{}^3P^e$ state of H^- (Refs. 6 and 7) were based upon a measurement of the radiation emitted in the decay process shown in Eq. (1). The present experiment complements the above work in that we tried to detect the H($1s$) decay product. Since the $2p^2\,{}^3P^e$ state very readily appears in variational calculations for H^-,[15–17] it is remarkable that all three experiments to detect its presence have failed. It may be that the cross section for the process

$$H^-(1s^2\,{}^1S)+Hg\rightarrow H^-(2p^2\,{}^3P)+Hg$$

is less than the upper limit of 10^{-20} cm^2 set by the present work. It is conceivable that the excited state was rapidly depopulated by the applied field of 1000–1500 V/cm, but this seems unlikely. The negative result casts doubt upon the identification of a stellar absorption feature[5] as arising from the $2p^2\,{}^3P^e$ state of H^-.

As a byproduct of this work, we have obtained the first absolute measurements of charge-transfer cross sections for hydrogen ions colliding with mercury. The cross-section ratios in Fig. 6 show an independence of scattering angle that is not shared by heavier ions. There is a need for further theoretical work to explain these results.

*Permanent address: Department of Physics, Lehigh University, Bethlehem, PA 18015.

[1]C. L. Pekeris, Phys. Rev. **126**, 1470 (1962).
[2]G. W. F. Drake, APEA J. **184**, 145 (1973), and earlier references therein.
[3]V. L. Jacobs, A. K. Bhatia, and A. Temkin, APEA J. **191**, 785 (1974).
[4]V. L. Jacobs, A. K. Bhatia, and A. Temkin, APEA J. **242**, 1278 (1980).
[5]S. R. Heap and P. Stecher, APEA J. **187**, L27 (1974).
[6]J. S. Risley, F. J. de Heer, and C. B. Kerkdijk, *Abstracts of the Papers of the Ninth International Conference on the Physics of Electronic and Atomic Collisions, Seattle, 1975,* edited by J. S. Risley and R. Gaballe (University of Washington, Seattle, 1975).
[7]G. Berry (private communication).
[8]H. Tawara and A. Russek, Rev. Mod. Phys. **45**, 178 (1973).
[9]T. J. Morgan and F. Eriksen, Phys. Rev. A **19**, 2185 (1979).
[10]T. J. Morgan and F. Eriksen, Phys. Rev. A **19**, 1448 (1979).
[11]B. Hird and H. C. Suk, Phys. Rev. A **14**, 928 (1976).
[12]A. van Wijngaarden and W. E. Baylis, Phys. Rev. A **7**, 937 (1973).
[13]A. van Wijngaarden, B. Miremadi, and W. E. Baylis, Can. J. Phys. **50**, 1938 (1972).
[14]E. W. Thomas, L. A. Leatherwood, and J. E. Harris, Phys. Rev. A **12**, 1835 (1975).
[15]J. Midtdal, Phys. Rev. **138**, A1010 (1965).
[16]G. W. F. Drake, Phys. Rev. Lett. **24**, 127 (1970).
[17]A. K. Bhatia, Phys. Rev. A **2**, 1667 (1970).